(Received 4 October 2023, Accepted 20 November 2023, Scheduled 26 November 2023)

A Freely Extendable Closely Packed Dual-Band MIMO Antenna for 5G Wireless Communication

Jinrong Su[1,*], Beijin Lin[1], Haipeng Dou[2], and Xinwei Chen[1]

[1] School of Physics and Electronic Engineering, Shanxi University, Shanxi 030006, China
[2] School of Information Engineering, Shanxi Vocational University of Engineering, Science and Technology, Jinzhong, China

ABSTRACT: In this paper, a freely extendable dual-band multiple-input multiple-output (MIMO) antenna for 5G wireless communication is proposed. The highlight of the antenna is that the 2-port array can be freely extended by repeating the radiating elements and decoupling structure periodically. A 2-port MIMO antenna is proposed firstly. It consists of two dual-band radiating elements placed side by side with edge-to-edge spacing of $0.08\lambda_0$. Then, a novel multiple bent split ring (MBSR) metamaterial (MTM) unit is designed. By adjusting the size, two kinds of units with single negative characteristics at two resonance points are obtained. By arranging the MBSR-MTM units cleverly between the two elements, dual-frequency decoupling is realized. Simulated and experimental results indicate that the antenna can operate at frequencies of 2.57∼2.62 GHz and 3.5∼3.6 GHz with the highest isolation of 30.2 dB and 44.5 dB, respectively. Additionally, the envelope correlation coefficient (ECC) is much smaller than 0.05, implying good diversity performance. Furthermore, simulated and experimental results show that the 2-port antenna can be freely extended to multiple-port MIMO antenna without any modification, and the isolation between different ports remains high. The antenna has a compact structure, low profile, and high isolation, providing an excellent choice for 5G wireless communication.

1. INTRODUCTION

The fast growth of the 5G wireless communication technology puts forward higher requirements for communication transmission rate and quality. Multiple-input multiple-output (MIMO) technology comes into being since it can effectively improve the channel capacity without additional bandwidth [1]. Simultaneously, to meet the requirements of device miniaturization and portability, the antenna size is constantly reduced, which results in enhanced mutual coupling. Thus, how to suppress the mutual coupling becomes a key problem in the MIMO antenna design.

Up to now, various methods to suppress coupling have been proposed, including polarization diversity [2, 3], using neutralization line [4], defective ground structure (DGS) [5, 6], introducing electromagnetic bandgap (EBG) structure [7], and arranging metamaterial (MTM) or metasurface (MS) based structure [8–17]. Polarization diversity can obtain high isolation without adding additional decoupling structure as proposed in [2] and [3]. Adding neutralization lines between radiation elements is also an effective method to reduce coupling. For example, in [4], two U-shaped neutralization lines are introduced to neutralize coupling current and the isolation reaches 25 dB. In some works, DGS are introduced by etching slots on the ground to suppress coupling as reported in [5] and [6]. In [7], a double-layer EBG structure is loaded on the ground between two monopoles, and isolation of 15 dB is obtained. Additionally, MTM or MS based decoupling methods are becoming popular. Split-ring resonators (SRRs) [8–10], complementary SRRs [11] or some other shape of resonators [12, 13] act as MTM or MS cells. The MTM or MS cells can be placed around [8] or between the radiation elements [14–17] or above the entire MIMO antenna [10, 13], and good isolation is obtained. The methods mentioned above can effectively reduce mutual coupling. However, it is worth noting that most of the MIMO antennas reported so far cannot be flexibly extended. In future applications of wireless communication systems, MIMO antennas need to be freely extended according to different system requirements [2].

This paper proposes a freely extendable dual-band MIMO antenna with high isolation. The antenna element is coaxial-fed concave-shaped patch. By placing two radiating elements side by side a 2-port MIMO antenna is formed. The edge-to-edge spacing is $0.08\lambda_0$(λ_0 is the free space wavelength corresponding to the lower resonant frequency). To suppress the mutual coupling, a novel multiple-bent split ring metamaterial (MBSR-MTM) unit is proposed. Single negative characteristics at two resonance points are obtained by adjusting the MBSR-MTM unit size. Dual-band decoupling is realized by placing the MTM units between the two radiating elements. In addition, the 2-port MIMO antenna can be freely extended into multiple-port by periodically repeating the radiation element and decoupling structure along x- or y-axis or both. The simulated and experimental results show that after extending, the operation bands remain the same and the isolation between ports still maintain a high level.

* Corresponding authors: Jinrong Su (sujinrong@sxu.edu.cn).

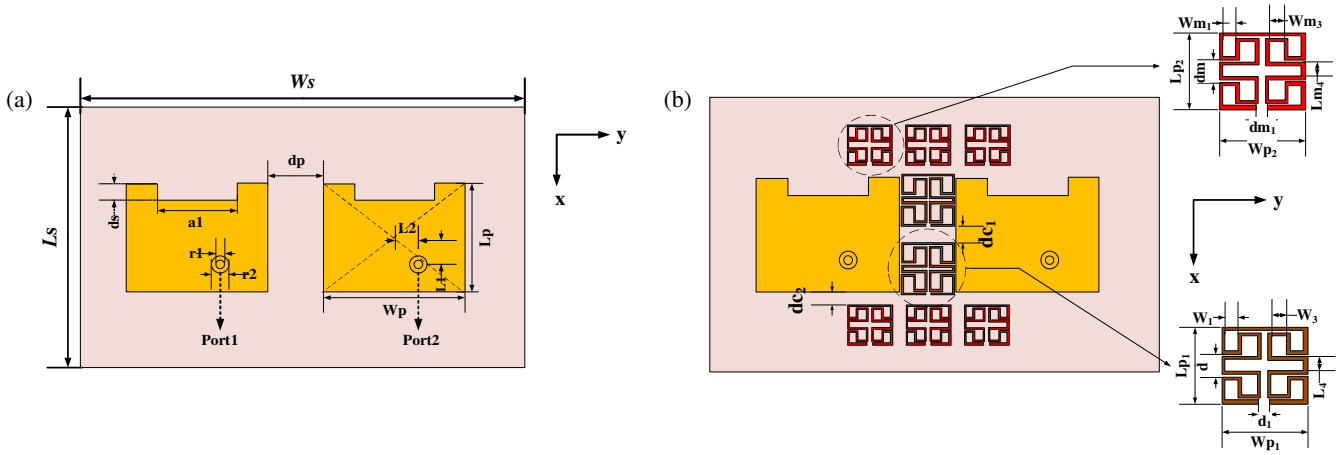

FIGURE 1. Antenna geometry (a) without and (b) with decoupling structure.

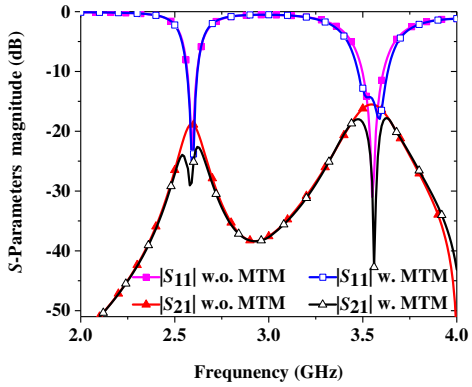

FIGURE 2. S-parameters with and without decoupling structure.

2. ANTENNA DESIGN AND ANALYSIS

2.1. Design of 2-Port MIMO Antenna

The initial 2-port MIMO antenna is constructed by placing two dual-band patch elements side-by-side, as depicted in Fig. 1(a). The edge-to-edge spacing is 0.08 λ_0. Dual-band is realized by adopting 50 Ω coaxial feed near the diagonal position of the rectangular radiation patch, and the resonant frequency is adjusted by introducing a slender rectangular slot at the upper part of the patch. Low-cost dielectric FR4 (thickness $h_s = 1.6$ mm, $\varepsilon_r = 0.02$, $\tan\delta = 4.4$) is chosen as substrate. The position (L_1, L_2) of the feeding point is calculated according to the formula [18]:

$$L_1 = -L_2 = 0.077\frac{c}{f\sqrt{\varepsilon_r}} \tag{1}$$

where f and c are the antenna resonant frequency and the speed of light, respectively. In order to reduce the mutual coupling, a novel multiple bent split ring metamaterial (MBSR-MTM) unit is proposed. Eight units in two sizes are printed between the two patches as illustrated in Fig. 1(b). The optimized geometrical parameters are list in Table 1.

ANSYS HFSS software is used to simulate and optimize the antennas. Fig. 2 shows S-parameters of the antennas before and after decoupling. The antenna can operate at 2.57∼2.62 GHz and 3.5∼3.61 GHz simultaneously. Besides, the isolation at the two resonant points of 2.58 GHz and 3.55 GHz is significantly improved by the decoupling structure, from −18.7 dB and −15.5 dB to −28.7 dB and −42.7 dB, respectively.

2.2. Decoupling Design of MIMO Antenna

Figure 3(a) shows the simulation setup of the MBSR-MTM unit (which is placed on an FR4 dielectric substrate with the same properties and thickness as the antenna). The top and bottom faces are set as perfect magnetic (PMC) boundary, and the front and back faces are set as perfect electric (PEC) boundary. Two wave port excitations are added on the left and right faces. In order to reduce coupling at two frequency bands, two kinds of MBSR-MTM with different dimensions are simulated and optimized. For simplicity, the larger and smaller ones are named MBSR-MTM-I and MBSR-MTM-II, respectively.

Figure 3(b) plots the simulated S-parameter of the MBSR-MTM units. They generate two stopbands at 2.61∼2.75 and 3.5–3.7 GHz, respectively. Besides, Fig. 3(c) shows the permittivity and permeability of the MBSR-MTM units. One can observe that at 2.5∼3.2 GHz for MTM-I and 3.4∼3.9 GHz for MTM-II, the real part of the permittivity is negative, and that of the permeability is positive. In a single-negative medium the propagation of energy is gradually attenuated. Therefore, the

TABLE 1. Dimensions of the proposed antenna.

Parameters	Dimensions (mm)	Parameters	Dimensions (mm)	Parameters	Dimensions (mm)
Ws	78	Ls	48	Wp	25
Lp	20	L_1	4.6	L_2	4.2
r_1	0.6	r_2	1.35	a_1	14.2
ds	3.1	dp	10	Wp_1	9.2
Lp_1	9	d_1	1	d	2
W_1	1.79	W_3	2	L_4	0.9
Wp_2	7.8	Lp_2	7	dm_1	1
dm	2	Wm_1	1.2	Wm_3	1.8
Lm_4	1.3	dc_1	3	dc_2	2.2

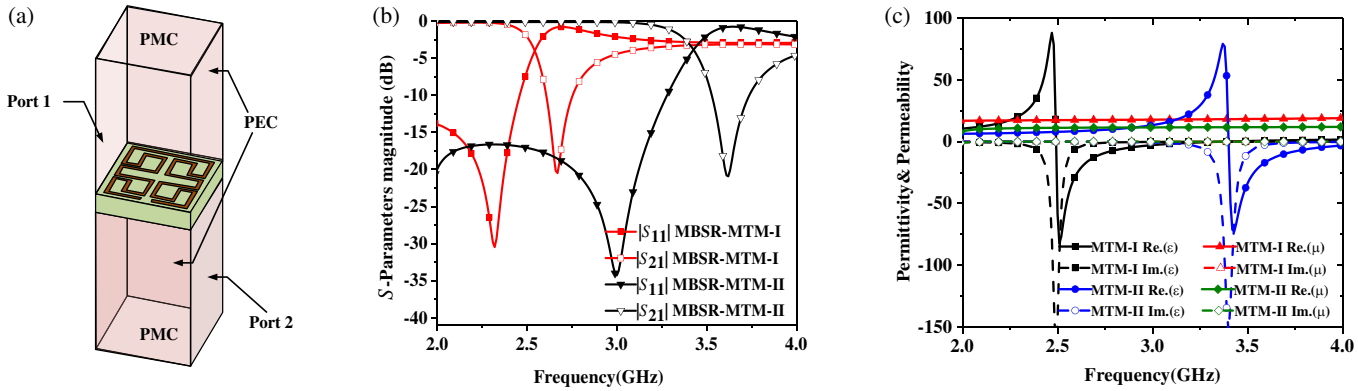

FIGURE 3. (a) Simulation setup, (b) S parameters, and (c) permittivity and permeability curves of MBSR-MTM metamaterial units.

MBSR-MTM units added between the two radiation patches is beneficial to suppress the mutual coupling.

To verify the decoupling effect of the MBSR-MTM structure, Fig. 4 gives the distributions of surface currents with and without the MBSR-MTM units. In simulation, port 1 is excited and port 2 terminated with 50 Ω load. One can observe that the surface currents coupled to port 2 are significantly reduced if the decoupling units are arranged. The currents originally coupled to port 2 concentrate to the MTM units in opposite directions, as shown by the black arrows in Figs. 4(b) and 4(d). The radiation from opposing currents cancels each other out, thus the coupling is reduced.

2.3. Extendibility of the Antenna

Since multiple-port MIMO antenna is beneficial for enhancing system channel capacity, and free extendibility will make it more flexible to be used in different systems, it is necessary to discuss the extendibility of the antenna. The following will take horizontal, vertical, and bidirectional extension as examples to illustrate its extendibility.

First, extendibility along the horizontal direction (y-axis) is verified. As shown in Fig. 5(a), a 3-port MIMO antenna is obtained by repeating the decoupling structure and element 2 along y-axis (or repeating element 1 and the decoupling structure along $-y$-axis). For simplicity, the MTM units are replaced with rectangular boxes. The edge-to-edge spacing between elements 2 and 3 is also 0.08 λ_0. Fig. 5(b) displays the simulated S-parameters of the 3-port MIMO antenna. The operation bands remain the same and the isolation is better than 20 dB. For example, at 2.58 and 3.55 GHz, $|S_{13}|$ is -23.7 and -33.6 dB, and $|S_{23}|$ is -31.8 and -34.9 dB, respectively.

Second, repeat the entire 2-port antenna along x-axis, and a 4-port antenna is achieved, as shown in Fig. 6(a). The edge-to-edge spacing between elements 1 and 3, dg, is 23.2 mm. Simulated S-parameter is shown in Fig. 6(b). One can see that the operation bands keep the same. Additionally, $|S_{ij}|$ ($i = 1$, 2, $j = 1 \sim 4$) are lower than -20 dB in both frequency bands, implying good coupling suppression performance.

The discussion above indicates that it is feasible to extend the 2-port antenna along x- and y-axes, respectively. Next, the extendibility along both directions simultaneously is verified. Take 8-port antenna for example, as described in Fig. 7, the decoupling structure and radiation element is repeated along y-axis twice to form 1×4 antenna array. Then repeat the entire array along x-axis and an 8-port antenna is achieved. In repetition, the edge-to-edge spacings keep the same as that of the 3-port and 4-port MIMO antennas above.

Figure 8 shows the simulated and measured S-parameters of the 8-port antenna. Considering the symmetry and reciprocity, only the results of $|S_{ij}|$ for $i = 1$ and 2, $j = 1$, 2, …8, and $i < j$ are shown here. It can be observed that the -10 dB impedance bands are 2.55∼2.63 GHz and 3.47∼3.62 GHz, which are nearly the same as that of the 2-port

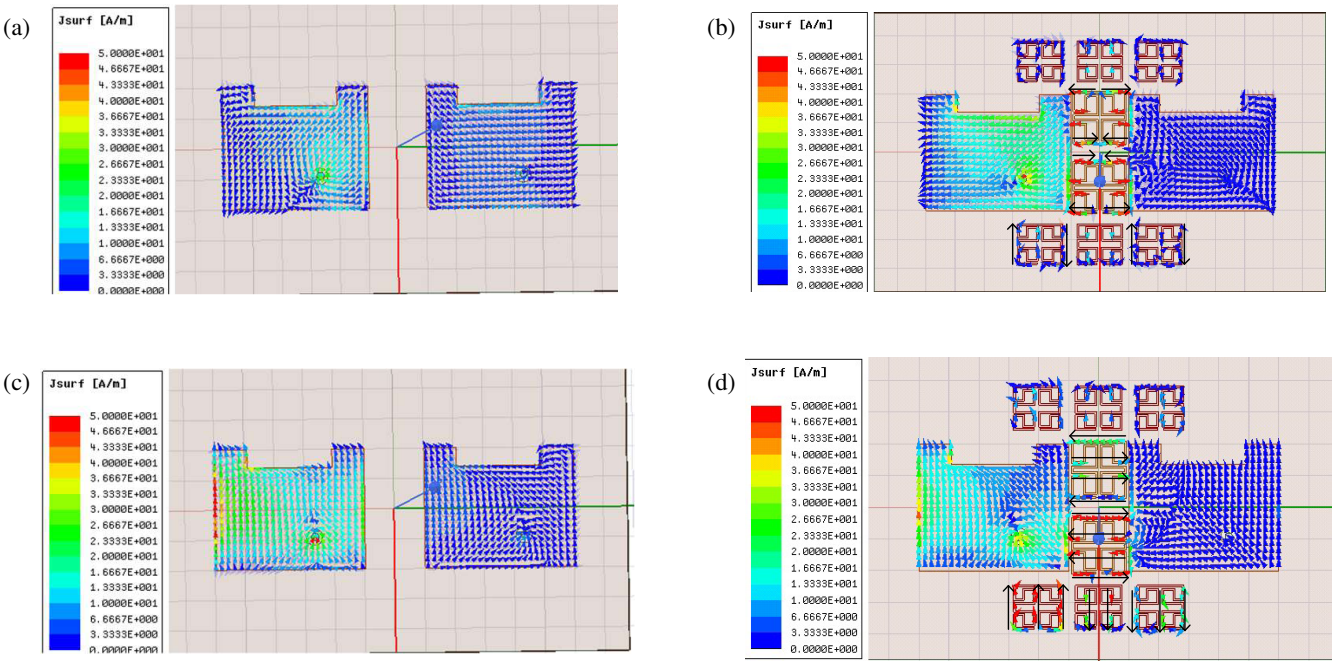

FIGURE 4. Current distributions before and after decoupling: (a) at 2.58 GHz, before decoupling (b) at 2.58 GHz, after decoupling (c) at 3.55 GHz, before decoupling (d) at 3.55 GHz, after decoupling.

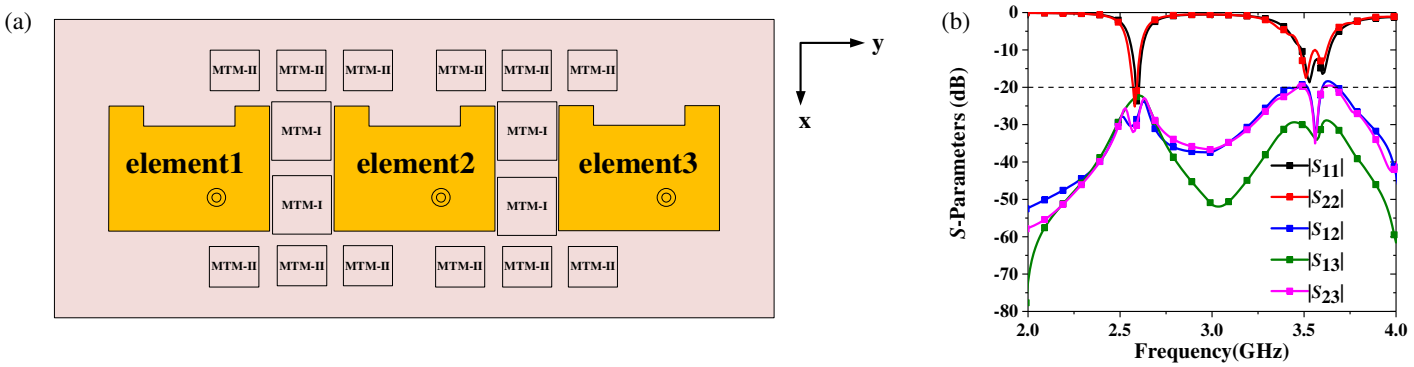

FIGURE 5. (a) Top view and (b) S-parameters of the 3-port MIMO antenna.

MIMO antenna. Besides, the transmission coefficients $|S_{ij}|$ $(i \neq j)$ at the two resonant points are lower than -20 dB. For example, at 2.6 GHz $|S_{15}|$ and $|S_{18}|$ are -21.5 and -34.7 dB, which are the largest and the smallest ones of the 12 curves of $|S_{ij}|$. At 3.55 GHz, the largest and smallest ones are $|S_{26}|$ and $|S_{16}|$, and the values are -22.1 and -42.5 dB, respectively. Therefore, the isolations between different ports of the 8-port MIMO antenna are high.

3. RESULTS AND DISCUSSIONS

The prototypes of the 2-port and 8-port antennas are fabricated, and Fig. 9 gives the photographs. S-parameters are measured using the Agilent N5222A vector network analyzer, and the radiation patterns are measured using Lab-Volt 8092 training system.

Figure 10 plots the simulated and measured S-parameters for the 2-port MIMO antenna. One can observe that the frequencies of the measured results shift toward low frequencies slightly compared with the simulation ones. The resonant points shift from 2.58 GHz and 3.55 GHz to 2.47 GHz and 3.5 GHz, respectively. Besides, the simulated and measured $S_{21}|$ at the corresponding frequencies are -28.7 and -42.7 dB, and -30.2 and -44.5 dB, respectively. The deviation between the simulation and experiment results is mainly caused by the accuracy of substrate dielectric constant and the accumulation of the fabrication tolerance.

Moreover, the measured S-parameters of the 8-port MIMO antenna are ploted in Fig. 8. There are similar frequency shifts as that of the 2-port ones. The largest and smallest experimental transmission coefficients at 2.6 GHz are -19.6 and -35.4 dB, and at 3.55 GHz are -25.8 and -44.1 dB, respectively.

Additionally, Fig. 11 depicts the simulated and experimental far-field radiation patterns of the 2-port MIMO antenna at 2.58 GHz and 3.55 GHz. The co-polarizations of the E- and H-planes are both approximately omnidirectional. The con-

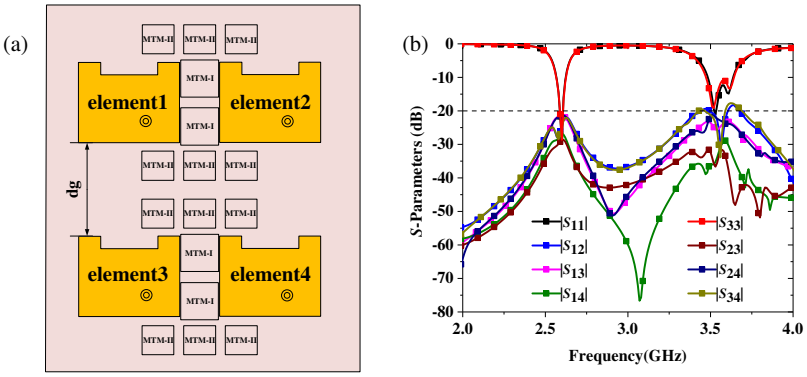

FIGURE 6. (a) Top view and (b) S-parameters of the 4-port MIMO antenna.

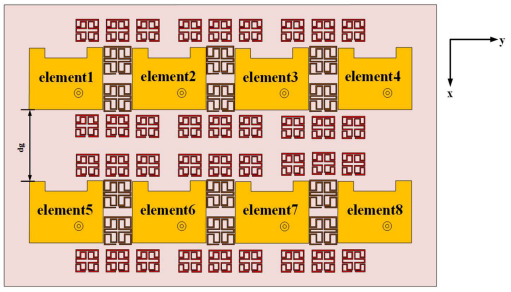

FIGURE 7. Top view of the 8-port MIMO antenna.

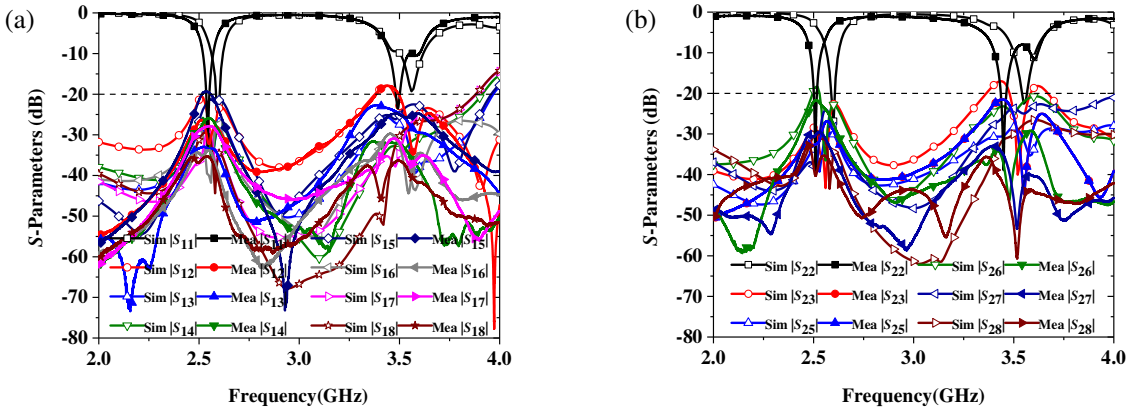

FIGURE 8. S-parameter curve of 8-port MIMO antenna: (a) $|S_{1j}|$, $j = 1, 2, \ldots 8$, and $i < j$. (b) $|S_{2j}|$, $j = 2, 3, 5, 6, 7, 8$, and $i < j$.

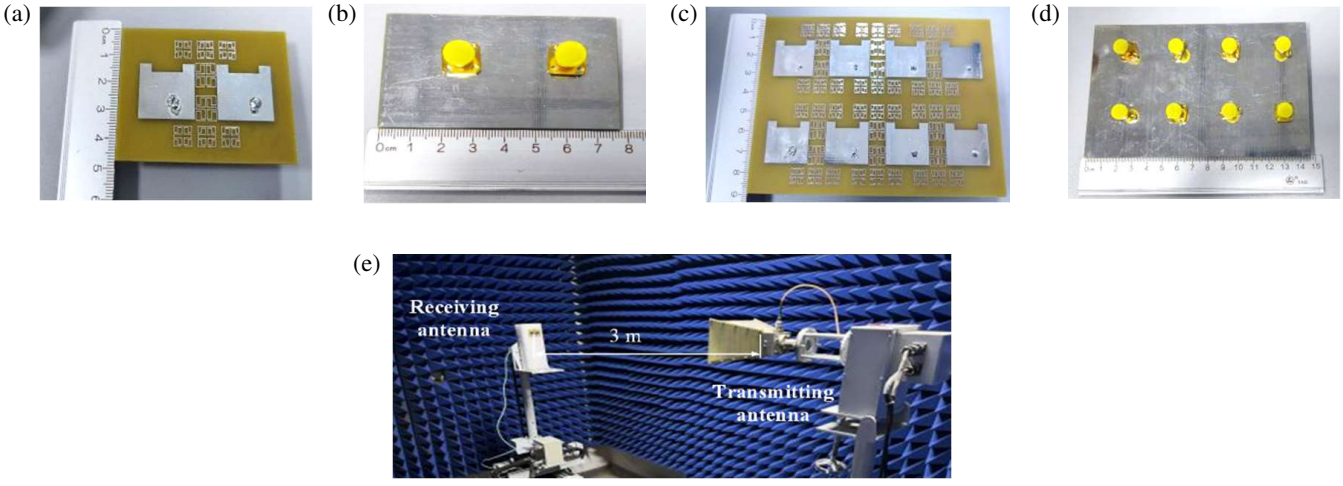

FIGURE 9. Antenna photographs and test environment: (a) top view and (b) bottom view of the 2-port antenna (c) top view and (d) bottom view of the 8-port antenna (e) test environment.

sistency between experimental and simulated results is good. Moreover, the peak gains of the antenna at the two resonant frequencies are 0.4 dB and 2.1 dB, respectively, which satisfy the requirements of 5G wireless communication system.

To verify the diversity performance of the proposed antenna, the envelope correlation coefficient (ECC), diversity gain (DG), total active reflection coefficient (TARC), and channel capacity loss (CCL) are calculated and analyzed. When those of 8-port array are calculated, for simplicity, results of three pairs of ports including ports 1 and 6, ports 1 and 5, and ports 2 and 5 are displayed because they have the maximum, minimum, and middle measured isolation. The ideal value of

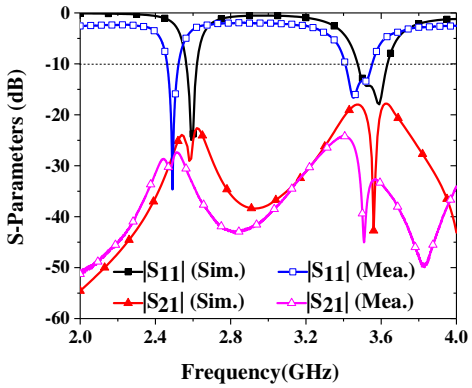

FIGURE 10. Simulated and measured S-parameters for the 2-port MIMO antenna.

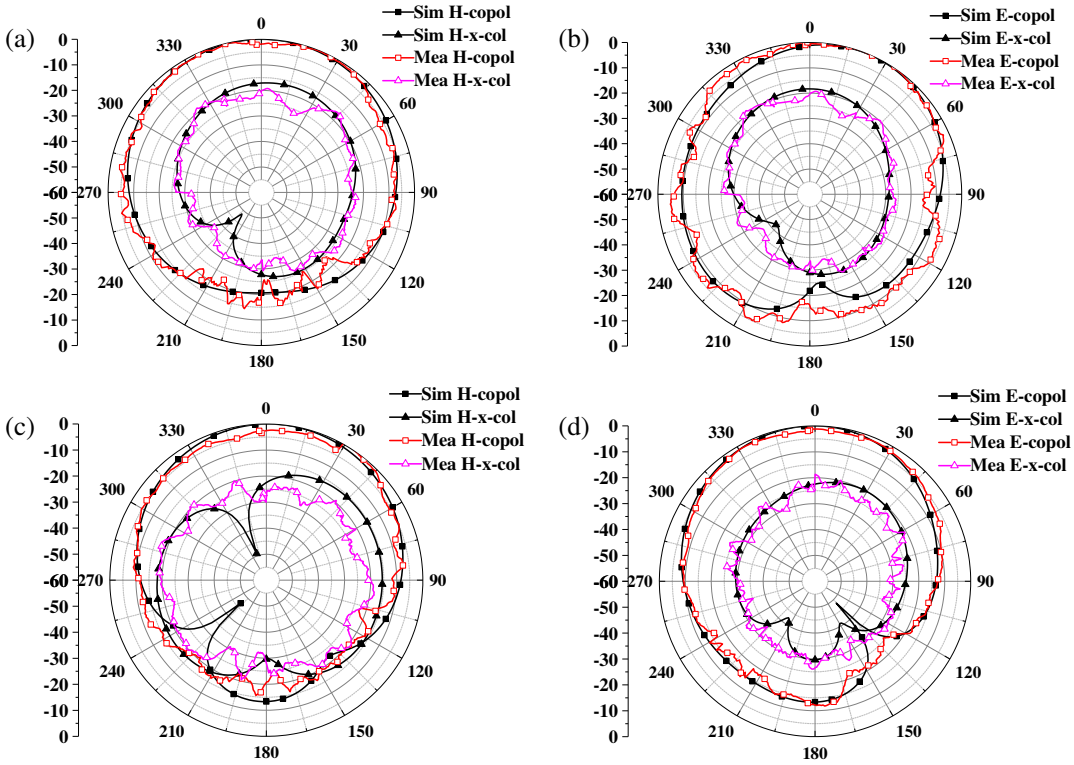

FIGURE 11. Radiation pattern of proposed MIMO antenna: (a) 2.58 GHz, H-plane (b) 2.58 GHz, E-plane (c) 3.55 GHz, H-plane (d) 3.55 GHz, E-plane.

DG is higher than 6 dB, and those of ECC, TARC, and CCL are smaller than 0.5, 0 dB, and 0.5 bit/s/Hz [19–21].

ECCs are calculated using the following formula [19]:

$$\rho_{eij} = \frac{\left|S_{ii}^{*}S_{ij} + S_{ji}^{*}S_{jj}\right|^{2}}{\left(1 - |S_{ii}|^{2} - |S_{ji}|^{2}\right)\left(1 - |S_{jj}|^{2} - |S_{ij}|^{2}\right)} \tag{2}$$

where * denotes complex conjugate. The DGs are calculated based on ECC according to [21]:

$$DG = 10\sqrt{1 - |ECC|^{2}} \tag{3}$$

The ECCs and DGs of 2-port and 8-port MIMO antennas are displayed in Fig. 12. One can observe that ECCs are less than 0.05, and DGs are above 9.9 dB in both operation bands, indicating good diversity performance.

Additionally, TARC is calculated using the following formula [20]:

$$TARC = \sqrt{\frac{(S_{ii} + S_{ij})^{2} + (S_{ji} + S_{jj})^{2}}{2}} \tag{4}$$

The results are shown in Fig. 13. At the two operation bands, the TARCs are lower than -10 dB for both the 2-port and 8-port MIMO antennas. Besides, the CCLs can be calculated according to the formulas [19]:

$$CCL = -\log_{2}\det\left(\psi^{R}\right) \tag{5}$$

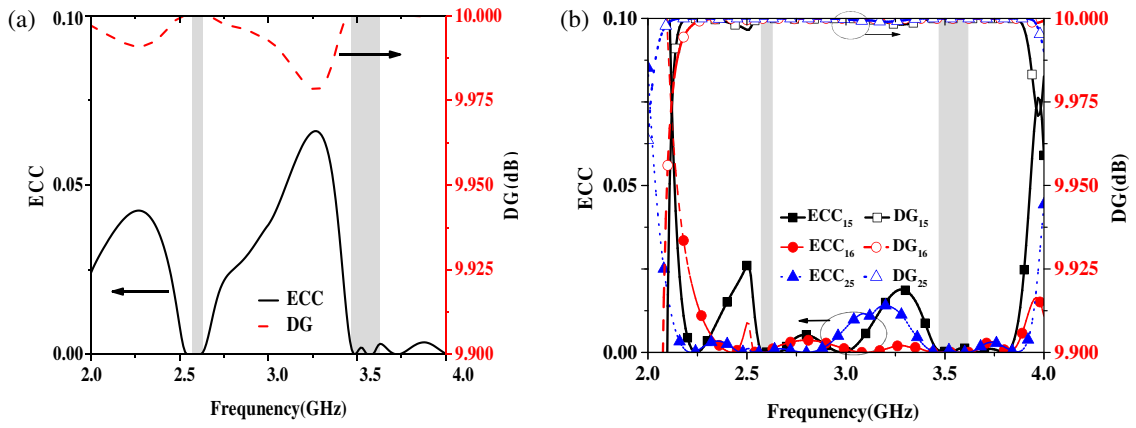

FIGURE 12. ECC and diversity gain of (a) 2-port and (b) 8-port MIMO antennas.

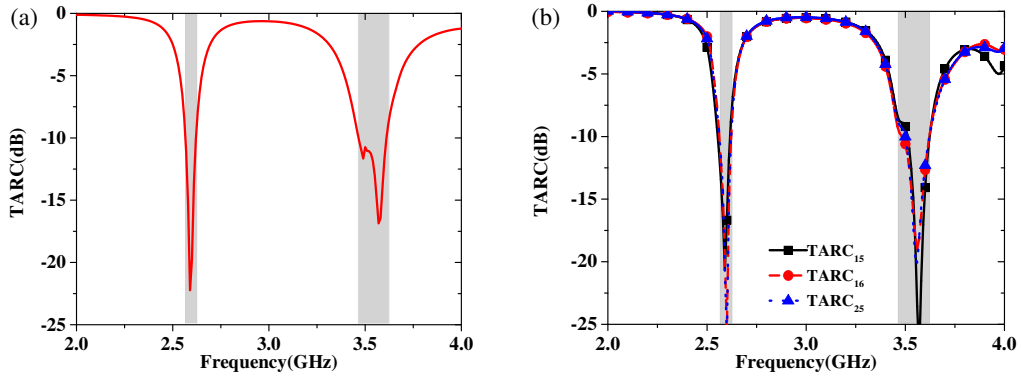

FIGURE 13. TARC of (a) 2-port and (b) 8-port MIMO antennas.

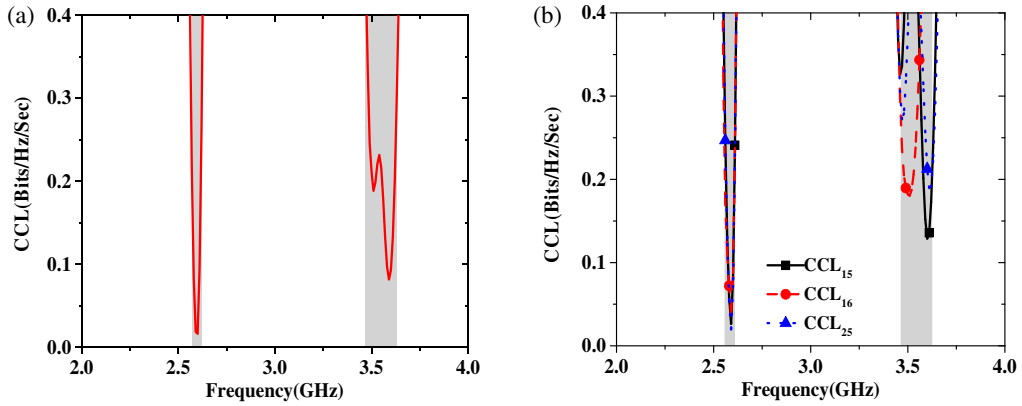

FIGURE 14. CCL of (a) 2-port and (b) 8-port MIMO antennas.

$$\psi^R = \begin{bmatrix} \rho_{11} & \rho_{12} \\ \rho_{21} & \rho_{22} \end{bmatrix} \quad (6)$$

$$\rho_{ii} = 1 - \left(|S_{ii}|^2 + |S_{ij}|^2 \right) \quad (7)$$

$$\rho_{ij} = -\left(S_{ii}^* \times S_{ij} + S_{ji}^* \times S_{jj} \right), \; i \text{ and } j = 1 \text{ or } 2 \quad (8)$$

The results of CCLs are illustrated in Fig. 14. One can observe that both antennas have CCL of less than 0.4 bits/Hz/sec in both operation bands.

To discuss the novelty of the proposed antennas, several previously reported compact MIMO antennas are compared with this work in Table 2. One can notice that the edge-to-edge spacing of this work is smaller than that of most of the antennas in the list (except [8, 10, 13, 17]). Meanwhile, compared with that in [8, 10, 13, 17], the antenna in this work has smaller overall size and higher isolation. Considering the extendibility and isolation enhancement, the antenna in this work has excellent comprehensive performance.

TABLE 2. Comparisons between the proposed 2-port MIMO antenna and the referenced works.

Reference	Antenna Size (mm^3)	Bandwidth (GHz)	edge-to-edge spacing (mm)	Isolation (dB)	Enhancement (dB)
[3]	$0.56\lambda_0 \times 0.56\lambda_0 \times 0.011\lambda_0$	2.1–20	$0.12\lambda_0$	-25	-
[7]	$0.6\lambda_0 \times 0.5\lambda_0 \times 0.015\lambda_0$	3–6	$0.15\lambda_0$	-15	5
[8]	$1.16\lambda_0 \times 0.91\lambda_0 \times 0.05\lambda_0$	5–6	$0.06\lambda_0$	-25	17
[9]	$0.32\lambda_0 \times 0.23\lambda_0 \times 0.01\lambda_0$	2–18	$0.083\lambda_0$	-25	15
[10]	$0.74\lambda_0 \times 0.48\lambda_0 \times 0.14\lambda_0$	5.58–6	$0.02\lambda_0$	-20	12
[10]	$0.74\lambda_0 \times 0.48\lambda_0 \times 0.14\lambda_0$	5.58–6	$0.02\lambda_0$	-20	12
[12]	$0.62\lambda_0 \times 0.41\lambda_0 \times 0.013\lambda_0$	2.4–2.48 & 5.15–5.85	$0.115\lambda_0$	-18 & -23	12 & 15
[13]	$1.25\lambda_0 \times 0.83\lambda_0 \times 0.148\lambda_0$	2.5–2.7 & 3.4–3.6	$0.008\lambda_0$	-34 & -28	26 & 14
[14]	$0.71\lambda_0 \times 0.53\lambda_0 \times 0.028\lambda_0$	5.15–5.4	$0.14\lambda_0$	-27.5	12.5
[15]	$0.57\lambda_0 \times 0.49\lambda_0 \times 0.08\lambda_0$	2.2–2.7 & 5.03–5.59	$0.098\lambda_0$	-24 & -29	13 & 9
[16]	$0.48\lambda_0 \times 0.42\lambda_0 \times 0.013\lambda_0$	2.36–2.4 & 5.2–5.36	$0.112\lambda_0$	-30 & -27	15 & 9
[17]	$0.4\lambda_0 \times 0.25\lambda_0 \times 0.017\lambda_0$	3.4–3.6	$0.045\lambda_0$	-25	15
proposed	$0.67\lambda_0 \times 0.41\lambda_0 \times 0.013\lambda_0$	2.56–2.62 & 3.48–3.63	$0.08\lambda_0$	-30.2 & -44.5	11.7 & 29.5

4. CONCLUSION

A freely extendable closely packed dual-band MIMO antenna with high isolation has been proposed in this paper. The antenna elements are arranged closely (edge-to-edge distance of $0.08\lambda_0$) and the size of 2-port antenna is $0.67\lambda_0 \times 0.41\lambda_0 \times 0.013\lambda_0$. MBSR-MTM units with single negative characteristic are designed to suppress the mutual coupling. Besides, the 2-port antenna can be extended into multiple ports array by repeating radiation element and decoupling structure periodically without additional modification. Furthermore, prototypes of 2-port and 8-port MIMO antennas are fabricated and tested. The results indicate that both antennas have isolation of higher than 20 dB at 2.6 and 3.5 GHz bands. Maximum experimental isolation of 30.2 and 44.5 dB and enhancement of 11.7 and 29.5 dB at the two bands are achieved. Also, ECC (< 0.05), DG (≈ 10 dB), TARC (< -10 dB) and CCL (< 0.4 bits/s/Hz) have been calculated to evaluate the MIMO antenna system. The excellent comprehensive performance including good radiation performance, low profile, easy processing, and freely extendibility makes the antenna a promising choice for 5G wireless communication systems.

ACKNOWLEDGEMENT

This research work was funded by the National Natural Science Foundation of China (62071282) and the Fundamental Research Program of Shanxi Province (202203021211295). The authors thank Hangzhou Jiepai Information Technology Company for their support to fabricate the antennas.

REFERENCES

[1] Kwon, U.-K., G.-H. Im, and J.-B. Lim, "MIMO spatial multiplexing technique with transmit diversity," *IEEE Signal Processing Letters*, Vol. 16, No. 7, 620–623, Jul. 2009.

[2] Sipal, D., M. P. Abegaonkar, and S. K. Koul, "Easily extendable compact planar UWB MIMO antenna array," *IEEE Antennas and Wireless Propagation Letters*, Vol. 16, 2328–2331, 2017.

[3] Rekha, V. S. D., P. Pardhasaradhi, B. T. P. Madhav, and Y. U. Devi, "Dual band notched orthogonal 4-element MIMO antenna with isolation for UWB applications," *IEEE Access*, Vol. 8, 145 871–145 880, 2020.

[4] Yu, Y., L. Yi, X. Liu, and Z. Gu, "Mutual coupling reduction of dual-frequency MIMO array with neutralization lines," in *2015 Asia-pacific Microwave Conference (APMC), Vols 1-3*, Dec. 06–09, 2015.

[5] Soltani, S., P. Lotfi, and R. D. Murch, "A dual-band multiport MIMO slot antenna for WLAN applications," *IEEE Antennas and Wireless Propagation Letters*, Vol. 16, 529–532, 2017.

[6] Wang, L., Z. Du, H. Yang, R. Ma, Y. Zhao, X. Cui, and X. Xi, "Compact UWB MIMO antenna with high isolation using fence-type decoupling structure," *IEEE Antennas and Wireless Propagation Letters*, Vol. 18, No. 8, 1641–1645, Aug. 2019.

[7] Li, Q., A. P. Feresidis, M. Mavridou, and P. S. Hall, "Miniaturized double-layer ebg structures for broadband mutual coupling reduction between UWB monopoles," *IEEE Transactions on Antennas and Propagation*, Vol. 63, No. 3, 1170–1173, Mar. 2015.

[8] Wang, Z., C. Li, Q. Wu, and Y. Yin, "A metasurface-based low-profile array decoupling technology to enhance isolation in MIMO antenna systems," *IEEE Access*, Vol. 8, 125 565–125 575, 2020.

[9] Sakli, H., C. Abdelhamid, C. Essid, and N. Sakli, "Metamaterial-based antenna performance enhancement for MIMO system applications," *IEEE Access*, Vol. 9, 38 546–38 556, 2021.

[10] Wang, Z., C. Li, and Y. Yin, "A meta-surface antenna array decoupling (MAAD) design to improve the isolation performance in a MIMO system," *IEEE Access*, Vol. 8, 61 797–61 805, 2020.

[11] Qamar, Z., U. Naeem, S. A. Khan, M. Chongcheawchamnan, and M. F. Shafique, "Mutual coupling reduction for high-performance densely packed patch antenna arrays on finite substrate," *IEEE Transactions on Antennas and Propagation*, Vol. 64, No. 5, 1653–1660, May 2016.

[12] Deng, J., J. Li, L. Zhao, and L. Guo, "A dual-band inverted-1 MIMO antenna with enhanced isolation for WLAN applications," *IEEE Antennas and Wireless Propagation Letters*, Vol. 16, 2270–2273, 2017.

[13] Liu, F., J. Guo, L. Zhao, G.-L. Huang, Y. Li, and Y. Yin, "Dual-band metasurface-based decoupling method for two closely packed dual-band antennas," *IEEE Transactions on Antennas and Propagation*, Vol. 68, No. 1, 552–557, Jan. 2020.

[14] Xia, Y., S. Luo, and Y. Li, "MIMO antenna array decoupling based on a metamaterial structure," in *Proceedings of The 2018*

IEEE 7th Asia-pacific Conference on Antennas and Propagation (APCAP), 383–384, Aug. 05–08, 2018.

[15] Cheng, Y., Z. Sun, W. Lu, and H. Zhu, "A novel compact dual-band MIMO antenna," in *Proceedings of 2014 3rd Asia-pacific Conference on Antennas and Propagation (APCAP 2014)*, 157–160, Jul. 26–29, 2014.

[16] Luo, S., Y. Li, and W. Shi, "A dual-frequency antenna array with mutual coupling reduction via metamaterial structures," in *2018 IEEE Antennas and Propagation Society International Symposium on Antennas and Propagation & USNC/URSI National Radio Science Meeting*, 1385–1386, Jul. 08–13, 2018.

[17] Shabbir, T., M. T. Islam, S. S. Al-Bawri, R. W. Aldhaheri, K. H. Alharbi, A. J. Aljohani, and R. Saleem, "16-port non-planar MIMO antenna system with near-zero-index (NZI) metamaterial decoupling structure for 5g applications," *IEEE Access*, Vol. 8, 157 946–157 958, 2020.

[18] Nakano, H. and K. Vichien, "Dual-frequency square patch antenna with rectangular notch," *Electronics Letters*, Vol. 25, No. 16, 1067–1068, 1989.

[19] Chen, H. N., J.-M. Song, and J.-D. Park, "A compact circularly polarized MIMO dielectric resonator antenna over electromagnetic band-gap surface for 5g applications," Vol. 7, 140 889–140 898, 2019.

[20] Chandel, R., A. K. Gautam, and K. Rambabu, "Tapered fed compact UWB mimo-diversity antenna with dual band-notched characteristics," *IEEE Transactions on Antennas and Propagation*, Vol. 66, No. 4, 1677–1684, 2018.

[21] Ahmad, S., S. Khan, B. Manzoor, M. Soruri, M. Alibakhshikenari, M. Dalarsson, and F. Falcone, "A compact cpw-fed ultra-wideband multi-input-multi-output (MIMO) antenna for wireless communication networks," *IEEE Access*, Vol. 10, 25 278–25 289, 2022.